pp. 1–14 (2019)

Computer modelling of initial platelet adhesion during microvascular thrombosis

A. V. Belyaev*

Abstract — Hemostasis is one of the most important protective mechanisms that functions to maintain vascular integrity and prevent bleeding. In arterial and microvascular circulation, where the near-wall shear stress is relatively high, the hemostatic response begins with aggregation of platelets on the injured endothelium or collagen. Regulation of hemostasis and thrombosis is immensely complex, as it depends on the blood cell adhesion and fluid dynamics. A possible regulatory mechanism relies on the coil-stretch transitions in a plasma protein — von Willebrand factor — that serves as a ligand to platelet adhesive membrane receptors. In this work, the initial stages of thrombus growth are studied using a 3D computer model that explicitly accounts for the shear-dependent vWf conformation.

Keywords: Computational biology, lattice Boltzmann, physiological flows, platelet adhesion, thrombosis

MSC 2010: 92C35, 76Z05

Adhesion of blood platelets is essential for thrombosis and hemostasis in arteries and microvessels, where the wall shear stress exerted by the flowing blood is relatively high [3, 5, 38, 57]. According to the current knowledge, the interactions between a membrane receptor of platelets (GPIb) and a plasma protein von Willebrand factor (vWf) is responsible for the initial platelet attachment to injury and aggregation in arterial hydrodynamic conditions. Von Willebrand factor (vWf) is one of the largest soluble macromolecules, as it is produced by endothelium in a form of chain-shaped concatamers — 'multimers' — that can be as long as 5-10 micrometers [37, 41, 43, 45]. These multimers play a key role in initial hemostasis and thrombosis, especially in the prevention of severe bleeding associated with high shear stress regions in the blood flow [30, 43, 47]. There is a number of mechanical features of vWf that provide its physiological functioning. First, it is the susceptibility to the local hydrodynamic forces. Multimeric structure of vWf is known to make the adhesion sensitive to hydrodynamic conditions, providing intensive platelet aggregation at the high shear rates [13, 29, 43, 47]. In a flowing viscous fluid this protein can change its conformation thus increasing the number of ad-

*Lomonosov Moscow State University, Moscow 119991, Russia.
E-mail: aleksey_belyaev@yahoo.com

This research was supported by the Russian Science Foundation (Project No. 17-71-10150).
The author acknowledges the grant from the Russian Science Foundation (Project No. 17-71-10150). The computational resources were provided by the Supercomputing Center of Moscow State University (supercomputers Lomonosov and Lomonosov-2).

hesive sites available for platelets [13, 43]. Second, the outstandingly big length of these proteins was shown to be mechanically favourable for catching [6] and holding platelets [7] on thrombogenic substrates (e.g., subendothelial collagen, injured endothelium, etc.). Third, the microscopic structure of this protein and mechanochemical transitions may regulate the adhesiveness of blood platelets depending on the drag forces and hydrodynamic conditions [2, 30]. Finally, the initial adhesion of platelets causes their activation and formation of stable aggregates called 'thrombi' [12, 29, 48]. Normally, the defensive role of these aggregates is to block leakages and damaged blood vessels. However, in some cases a thrombus can obstruct the blood vessel, dangerously limiting the blood circulation and causing diseases (deep vein thrombosis, thrombotic thrombocytopenic purpura) and emergency conditions, such as stroke [12,26,31]. On the other hand, deficiency or dysfunctions of one (or several) components of cellular hemostatic response cause bleeding that is also dangerous for the organism. For instance, von Willebrand disease may be encountered if the vWf multimers are either too short, or limited in number (concentration), or are less adhesive to platelets than necessary [17,47]. Apparently, the adhesive system platelet-vWf is naturally 'tuned' to work in specific hydrodynamic conditions. If some parameters of this system are altered by internal (e.g., gene mutation) or external factors (e.g., acquired VWD syndrome), the hemostasis turns into either vascular occlusion or bleeding. In order to obtain a deeper understanding of the regulation of hemostasis and thrombosis, the physical mechanisms of these disorders need to be described and quantified in terms of physics and mathematics. The complexity of platelet aggregation and activation during thrombosis makes it a challenging goal for computational modelling [8], and several methods have been proposed so far. Whereas continuous models [5, 23, 49, 52, 53, 56] describe macroscale dynamics of platelet concentrations, many aspects of platelet adhesion and platelet-vWf interactions are better understood if they are modelled as discrete objects. Modelling explicitly the transport, activation, and adhesion of platelets is crucial for predicting thrombus formation and growth following a thrombotic event in normal or pathological conditions. Discrete methods include coarse-grained approaches [22,34,53,58] and high-resolution cell models [7,32,33,35,39,40,46,55] each having its own advantages and limitations [8].

The present paper reports a 3D computer model of the initial platelet adhesion to injury in arterial flow conditions (shear rates ¿ 1000 s^{-1}). The discrete approach has been chosen for the purposes of the reported study: the cells and proteins are modelled explicitly. The structure of the paper is as follows: first, the model is described, then the obtained results are presented, and the discussions of the results and possible future directions are given.

1. Materials and methods

In this work, the dynamics of platelet recruitment from the flowing blood to the injury was investigated by the means of computer simulations. The injury was represented by a number of polymer ligands (vWf multimers) attached to a plane surface.

The system was represented by a rectangular simulation box $b_x \times b_y \times b_z$ filled with a viscous fluid. Plane impenetrable no-slip boundaries were introduced at $z = 0$ and $z = b_z$. The blood cells (platelets and RBCs) were also introduced explicitly as deformable objects that were able to interact with each other, with polymers, and with the fluid. The physical model of these interactions was governed by a set of prescribed forces and constraints. The numerical method was based on a combination of the Lattice Boltzmann method (LBM) [50] with the Lagrangian Particle Dynamics (LPD) [18]. The model consists of three principal components: viscous fluid (blood plasma), blood cells, and the von Willebrand factor multimers (polymers). The description of each component is presented further in this section. In most simulations the following scales for length, force, and time were used: $[L] = 10^{-6}$ m, $[F] = 10^{-9}$ N, $[t] = 10^{-4}$ s. The physical parameters were non-dimensionalized according to this system of units.

The presented study is an extension of our previous works [6, 7]. A number of new features have been introduced, including the red blood cells with their mechanical properties tuned up in accordance with the experiments. Another modification important to mention is the introduction of the individual friction coefficients (i.e., hydrodynamic coupling coefficients) for each type of objects in the simulated system, that allows a precise tuning of the hydrodynamic forces and torques.

1.1. Fluid model

Continuum representation was used for the modelling of blood plasma, and Lattice Boltzmann method (LBM) was used to calculate fluid velocity in the simulation box. LBM is used as a fast solver for hydrodynamic equations, that inherits from lattice gas automata simulations [50]. The method rests upon the Boltzmann's kinetic equation that describes spacial-temporal changes of a one-particle distribution function $f(\mathbf{x}, \mathbf{u}, t)$:

$$\frac{\partial f}{\partial t} + \mathbf{u} \cdot \frac{\partial f}{\partial \mathbf{x}} + \frac{\mathbf{F}}{m} \cdot \frac{\partial f}{\partial \mathbf{u}} = \left(\frac{\partial f}{\partial t} \right)_{\text{coll}} \tag{1.1}$$

where the term in the right-hand side is the collision integral dependent on velocities of the collided particles before and after the collision.

A discretization scheme D3Q19 was used in this work, i.e., the fluid is treated as packets of fluid particles moving from one node to a neighbouring node of a 3D periodic cubic grid in 19 possible directions. A regular mesh of Eulerian spacial sites $\{\mathbf{x}\}$ with constant spacing $\Delta x = [L]$ was introduced, as well as a set of discrete microscopic velocities $\{\mathbf{c}_i\}$. The discretized distribution function $f_i(\mathbf{x}, t)$ obeys the following equation:

$$f_i(\mathbf{x} + \mathbf{c}_i \Delta t, t + \Delta t) = f_i(\mathbf{x}, t) + \Omega_i(\mathbf{x}, t) \tag{1.2}$$

and the evolution of the system could be found by the consequent iterations. Here

$f_i(\mathbf{x},t) \equiv f(\mathbf{x},\mathbf{c}_i,t)$ and

$$\mathbf{c}_i = c \times \begin{cases} (0,0,0), & i=0 \\ (\pm1,0,0),(0,\pm1,0),(0,0,\pm1), & i=1,2,\ldots,6 \\ (\pm1,\pm1,0),(0,\pm1,\pm1),(\pm1,0,\pm1), & i=7,8,\ldots,18. \end{cases} \tag{1.3}$$

The collision operator $\Omega_i(\mathbf{x},t)$ defines the rheological behaviour of the modelled fluid. For a viscous incompressible fluid a single-relaxation time approximation (or Bhatnagar–Gross–Krook approximation) has been proven to precisely reproduce the hydrodynamics for low Reynolds and Mach numbers [14, 35, 42, 50]:

$$\Omega_i(\mathbf{x},t) = -\frac{1}{\tau}(f_i(\mathbf{x},t) - f_i^{\mathrm{eq}}(\mathbf{x},t)). \tag{1.4}$$

The equilibrium distribution function $f_i^{\mathrm{eq}}(\mathbf{x},t)$ corresponds to the series expansion of Maxwell–Boltzmann distribution for small velocities [14, 50]. The zeroth and first moments of the distribution function give fluid density ρ and macroscopic fluid velocity $\mathbf{v}$ according to

$$\rho = \sum_i f_i, \quad \rho\mathbf{v} = \sum_i f_i \mathbf{c}_i. \tag{1.5}$$

A single relaxation time $\tau = 1/2 + \nu/(c_s^2 \Delta t)$ was used for the collision step, where $c_s^2 = (\Delta x/\Delta t)^2/3$ is the lattice speed of sound. For setting up the no-slip hydrodynamic boundaries the 'link bounce back' method was used [18].

The model allows one to simulate the platelet adhesion in presence of the plane shear flow (Couette flow) or Poiseuille (pressure-driven) flow.

1.2. Cell model

The platelets and red blood cells (RBCs) were represented by a triangular mesh of Lagrangian surface points (LSPs). For the description of the platelet membrane dynamics we use the coupling between the fluid and the immersed objects (platelets) [10, 15, 16]. Particle dynamics approach has been used to simulate the motion of LSPs. The position $\mathbf{r}_{\mathrm{LSP}}$ and the velocity $\mathbf{v}_{\mathrm{LSP}}$ of each LSP were found from the solution of the following differential equations:

$$\frac{\mathrm{d}\mathbf{v}_{\mathrm{LSP}}}{\mathrm{d}t} = \frac{\sum_i \mathbf{F}_i}{m}, \quad \frac{\mathrm{d}\mathbf{r}_{\mathrm{LSP}}}{\mathrm{d}t} = \mathbf{v}_{\mathrm{LSP}} \tag{1.6}$$

where $\sum_i \mathbf{F}_i = \mathbf{F}_{\mathrm{elast}} + \mathbf{F}_{\mathrm{int}} + \mathbf{F}_{\mathrm{visc}}$ is the total force exerted on the ith LSP. It consists of the elastic forces from neighbouring particles in the membrane of the same cell (bonded interactions), the forces of non-bonded interactions with other cells, boundaries and polymers and viscous (drag) forces from the fluid.

The elastic model of each blood cell accounted for stretching elasticity, bending rigidity, conservation of volume and surface [16]: $\mathbf{F}_{\mathrm{elast}} = \mathbf{F}_{\mathrm{sp}} + \mathbf{F}_{\mathrm{b}} + \mathbf{F}_{\mathrm{a}} + \mathbf{F}_{\mathrm{v}}$. The

elastic force applied to the membrane points in the case of stretching (compression) of mesh edges is given by neo-Hookean law:

$$\mathbf{F}_{\mathrm{sp}} = k_s \frac{\lambda^{1/2} + \lambda^{-5/2}}{\lambda + \lambda^{-3}} \frac{\Delta l}{l_0} \mathbf{n} \tag{1.7}$$

where $\Delta l = l - l_0$ is the spring elongation relative to its equilibrium length l_0, $\lambda = l/l_0$, k_s is the stretching spring constant, and $\mathbf{n}$ is the unit vector pointing from one membrane point at another.

The bending elasticity force was meant to provide equilibrium angle ϑ_0 between two adjacent mesh triangles:

$$\mathbf{F}_{\mathrm{b}} = k_b \frac{\Delta\vartheta}{\vartheta_0} \mathbf{n}_b \tag{1.8}$$

where $\mathbf{n}_b$ is the unit vector normal to the triangle (pointing at the exterior of the capsule), $\Delta\vartheta$ is the angle deviation from ϑ_0, k_b is the bending elasticity constant. This force was applied to the vertex not belonging to the common edge of adjacent triangles. The opposite force divided by two was applied to the two vertices lying on the common edge.

The surface conservation force applied to the mesh nodes for maintaining the surface area of each mesh triangle is

$$\mathbf{F}_{\mathrm{a}} = -k_{\mathrm{al}} \frac{\Delta S_i}{(S_i^0)^{0.5}} \mathbf{w} - k_{\mathrm{ag}} \frac{\Delta S_g}{S_g^0} \mathbf{w} \tag{1.9}$$

where $\Delta S_i = S_i - S_i^0$ is the change of the ith mesh triangle area, $\mathbf{w}$ is a unit vector pointing from the centroid of the triangle at the vertex, k_{al} and k_{ag} are the coefficients. Finally, the volume conservation force is given by

$$\mathbf{F}_{\mathrm{v}} = -k_v \frac{\Delta V}{V_0} S_i \mathbf{n}_b \tag{1.10}$$

where $\Delta V = V - V_0$ is the capsule volume change, k_v is the coefficient of volume conservation. The force $\mathbf{F}_{\mathrm{v}}$ has been calculated for each ith triangle with area S_i and has been evenly distributed over the vertices of this triangle.

Each platelet consisted of 126 LSPs, and each RBC contained 304 LSPs on its membrane (see Fig. 1). The following dimensionless elastic parameters were used for the deformable RBCs with the conservation of membrane surface and volume: $k_s = 0.7$, $k_b = 0.1$, $k_{\mathrm{al}} = 1.0$, $k_{\mathrm{ag}} = 1.0$, and $k_v = 1.0$. The platelets, to the contrast, were assumed non-deformable, with $k_s = 5.0$, $k_b = 0.1$, $k_{\mathrm{al}} = 1.0$, $k_{\mathrm{ag}} = 1.0$, and $k_v = 1.0$.

It is important to note that the model allows one to use two different time-steps for the fluid solver and for the particle solver: $\Delta t_{LB} = N \cdot \Delta t_p$, where N is an integer. For the sake of computational efficiency, $N = 10$ was used in the majority of simulation runs. But in order to archive a higher accuracy at arterial shear rates ($> 2000\ \mathrm{s}^{-1}$) this value was set to $N = 2$. Dimensionless time-step was $\Delta t_p = 0.01$, providing the tradeoff between computational efficiency and accuracy. Any further decrease of Δt_p did not result in any detectable changes of the simulation results.

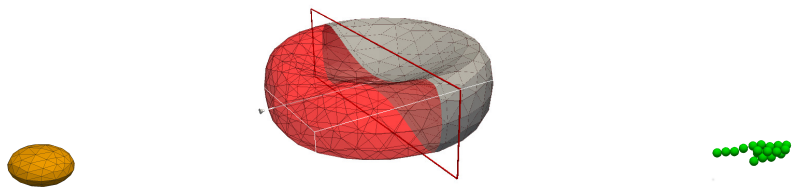

(a) (b) (c)

Figure 1. Particular components of the model (all panels are to scale): (a) a platelet, (b) a red blood cell (RBC) with its biconcave cross-section and (c) a polymer (i.e., von Willebrand factor multimer). The platelet is modelled as an oblate spheroid with aspect ratio 1:2 and the longer radius 1 μm. The diameter of the RBC is 8 μm. The size of the polymer depends on the number of monomers N_{mono}.

1.3. Polymer model

The vWf multimers were represented by the ball-and-spring free-jointed model of a polymer immersed into a viscous fluid. Finitely Extensible Non-linear Elastic (FENE) potential was used to describe bonded interactions between monomers in the chain:

$$U_{\text{FENE}} = -\frac{1}{2}K(\Delta r_{\max})^2 \ln\left[1 - \left(\frac{r - r_0}{\Delta r_{\max}}\right)^2\right] \tag{1.11}$$

with $r_0 = 2a$, monomer radius $a = 0.05$ μm. The stiffness of the chain $K = 0.04$ nN/μm and maximal extension of a bond $\Delta r_{\max} = 0.3$ μm were obtained by fitting the experimental force-distance plots obtained experimentally for vWf-dimer by its extension with an atomic-force microscope [36]. The number of monomers in the chain was varied from 10 to 50, corresponding to the full (extended) length in the range from 1 to 5 microns. The choice of sizes for the multimers was based on the experimentally measured mean length of healthy vWf multimers [47]. The role of vWf length in the promotion of platelet adhesion has been reported in a recent paper [7].

1.4. Coupling between the particles and fluid

The coupling between the particles and fluid was achieved via Ahlrichs and Dunweg's point coupling method with thermal fluctuations [1, 18, 28]. According to this approach, a viscous-like force acting between LB lattice nodes and membrane surface points was introduced. This force was taken to be proportional to the difference of the membrane point velocity v and the local fluid velocity u derived from the LB, $F_{\text{visc}} = -\xi(v - u)$. The opposite force was transferred back to the fluid. The parameter of friction ξ was adjusted from a special calibration procedure [4, 10] individually for each kind of cells: $\xi_{\text{plt}} = 0.43 \cdot 10^{-9}$ N/(m/s) and $\xi_{\text{RBC}} = 0.1 \cdot 10^{-6}$ N/(m/s). The validation of cell-fluid coupling for platelets was based on the calculations of drag forces and torques experienced by a platelet in a shear flow near a plane wall. It can be found in prior works [7, 10]. This method is appropriate for solid cell

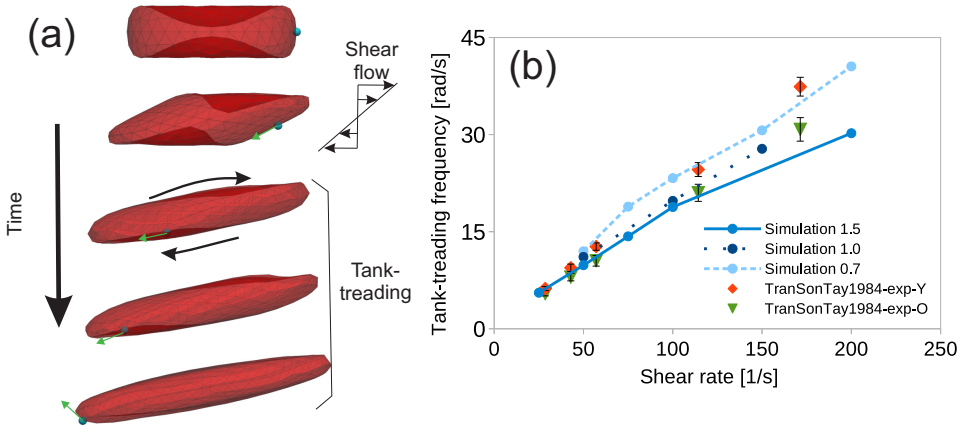

Figure 2. Validation of the constitutive model of RBCs and determination of the friction coefficient ξ_{RBC}. (a) Simulated tank treading motion of a red blood cell in a plane shear flow ($\dot{\gamma} = 100$ s^{-1}). A cyan-colored marker moves tangentially to the RBC's surface, while the cell maintains its inclined orientation. The frequency of such a tank-treading motion was measured as $2\pi/T$, where T is a period of marker's cyclic motion. (b) The frequency of the tank-treading motions of RBCs as a function of the shear rate $\dot{\gamma}$ in our simulations (circles with lines) and in the experiments by Tran-Son-Tay et al. [54] (diamonds correspond to the young RBCs and triangles to the old ones). The digits in the legend correspond to the friction coefficient ξ_{RBC} in dimensionless units.

of spherical or elliptical shape, for which the analytical expressions for drag coefficients are known. An alternative approach was used for deformable RBCs: the calibration of friction coefficient was done by measuring the tank-treading frequency ω_{tt} of RBCs in a plane shear flow (see Fig. 2). The value of ξ_{RBC} was adjusted so that ω_{tt} in the simulations agrees with the experimental observations [54].

A similar approach was used for the coupling between the polymers and the fluid. For each monomer, the hydrodynamic coupling coefficient can be determined theoretically from the Stokes's law $\xi_{\mathrm{vwf}} = 6\pi\mu r_h$. Theoretical value calculated in [6] reads $\xi_{\mathrm{vwf}} \approx 0.5$ nN/(m/s), thus in dimensionless units 0.005 is a reasonable approximation. Precise tuning of this parameter based on experimental data by [24, 43] gives a similar result.

1.5. Interactions

The non-bonded interactions were presented in the model by potential forces $\mathbf{F}_{\mathrm{int}} = -\nabla \sum_k U_k$. The adhesive interactions between vWf and the platelet are modelled via tunable Morse potential (truncated and shifted):

$$U_{\mathrm{vwf-plt}} = A_{\mathrm{vwf-plt}} \cdot \left[\left(1 - \mathrm{e}^{-\alpha(r-a)} \right)^2 - 1 \right] \tag{1.12}$$

where amplitude of potential is related to bond stiffness as $A_{\mathrm{vwf-plt}} = K_e/(2\alpha^2)$, $\alpha = 100\ \mu\mathrm{m}^{-1}$. The adhesive force depends on the distance r between the center of a monomer and the closest Lagrangian point on the platelet surface. The value

$A_{\mathrm{vwf-plt}}$ was varied in the range from $6.25kT$ to $125kT$. From experiments [30] it is known that healthy vWf-GPIb bond stiffness $K_e \approx 1$ nN/μm, that corresponds to $A_{\mathrm{vwf-plt}} = 12.5\ kT$.

Polymer-solvent interactions were introduced as an effective attraction between monomers, and the potentials and parameters were taken from [43]. The Lennard-Jones potential (truncated at $r = 1.2r_0$ and shifted)

$$U_{\mathrm{vwf-vwf}} = 4\varepsilon \left[\left(\frac{\sigma}{r}\right)^{12} - \left(\frac{\sigma}{r}\right)^{6} \right] \tag{1.13}$$

with $\sigma = 2^{-1/6} r_0$.

Soft sphere short-range repulsion was introduced $U_{\mathrm{rep}} = 10^{-3} \cdot (r - r_s)^{-n}$ between all particles belonging to different cells, and the same potential was used to make cells and walls impenetrable to polymers. The index was set to $n = 2$ for cells and $n = 1.2$ for the polymers. The off-set distance was introduced to avoid singularities: $r_s = 0.2$. The cutoff radius was $r_{\mathrm{cut}} = 0.3$ for cell-wall interaction, 0.8 for cell-cell interaction and $r_{\mathrm{cut}} = 2a = 0.1$ for the polymers.

Before each simulation run, the polymers multimers were attached to the bottom surface of the simulation box and equilibrated. The blood cells (platelets) were placed near the wall at a certain distance in the begging of each run. The density and size of attached vWf multimers were varied during this research.

2. Numerical results

The first set of simulation data was obtained by immersing the individual polymer in a plane shear flow (or Couette flow). The goal of this stage of the study was to ensure that the chosen model of the polymer reproduces the physico-mechanical properties of the von Willebrand factor multimers. The protocol of the numerical experiments as follows. The polymer was initially placed in the center of the simulation box by a random-walk procedure. Then it remained in the quiescent fluid for 1000 ms for equilibration. After that the shear rate was imposed in the fluid by setting the opposite velocities at $z = 0$ and $z = b_z$ boundaries. The shearing was on during another 1000 ms of the simulation. After that, the shearing was turned off and the polymer was left in the resting fluid for another 1000 ms.

The results presented in Fig. 3 indeed demonstrate that the polymer is sensitive to the local shear stress in the fluid. At low shear rates $\dot{\gamma} < 5000\ \mathrm{s}^{-1}$ the polymers remained in the conformation of a compact globule. At $\dot{\gamma}_{\mathrm{cr}} \approx 5000\ \mathrm{s}^{-1}$ shear-induced stretching transition takes place and at higher shear rates. It is seen in Fig. 3b–3d that the polymer returned to its compact conformation after the fluid flow has been turned off. The extension of the polymer in the direction of the shear flow was measured and averaged during the shearing time. Figure 3e shows that the model used in the present work gives reasonably correct results as compared to other authors [43]. Here we also conclude that the longer vWf multimers are more susceptible to the quality of the solvent, as the decrease of ε leads to a more pronounced increase of $R_{\mathrm{ext}}/(2aN_{\mathrm{mono}})$ for 50 monomers, than for 20 monomers.

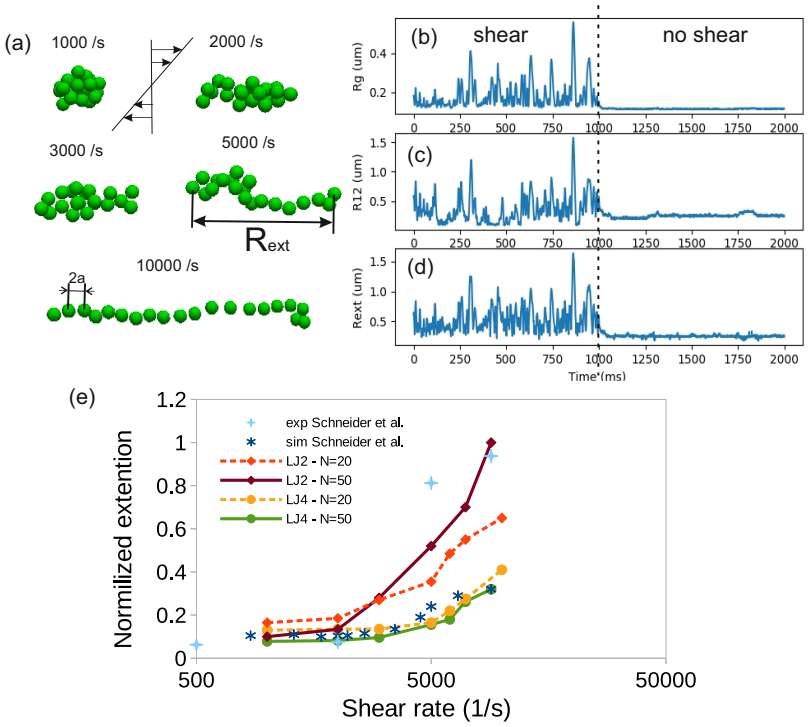

Figure 3. The dynamics of an individual vWf multimer in the shear (Couette) flow. (a) Simulation snapshots demonstrating the shape and size of the polymer at different shear rates. (b) The plot of the gyration radius R_g of the polymer as a function of time during the shearing simulation at shear rate $\dot{\gamma} = 7000$ s^{-1}, $\varepsilon = 4kT$, $N_{\text{mono}} = 20$, $\xi_{\text{VWF}} = 0.005$. (c-d) The plots of the end-to-end distance R_{12} and polymer extension along the shear direction R_{ext}. The parameters are the same as in the panel (b). (e) The dependency of the normalized polymer extension $R_{\text{ext}}/(2aN_{\text{mono}})$ as a function of the shear rate for different vWf-solvent interaction parameter (lines with diamonds correspond to $\varepsilon = 2\ kT$ and with circles — to $\varepsilon = 4\ kT$) and different polymer length ($N_{\text{mono}} = 20$ for dashed lines and 50 for solid lines). The stars and the asterisks correspond to experimental and simulation results reported by Schneider et al. [43]: the experimental results were scaled to the contour length of the vWf assuming that $N_{\text{mono}} = 100$ in their experiments, the simulation results were digitized from their plots without any additional assumptions.

The next set of simulations was devoted to the whole-blood flow in a plane-parallel (microfluidic) channel. The simulation box had the dimensions $32 \times 16 \times 16\ \mu\text{m}^3$, thus reproducing microvascular hemodynamic conditions. The pressure-driven Poiseuille flow was set by defining the constant pressure difference in x-direction. The parallel calculations were performed by 8-core processors for each simulation run. The RBCs were initially placed in ordered positions in the bulk fluid, and the platelets were placed near the wall. A number of 50 vWf multimers ($N_{\text{mono}} = 20$) was attached to the bottom wall of the system in its central part (see Fig.4). The first particle of each polymer had fixed coordinates, while the others were allowed to move freely in response to external forces. In case of $\dot{\gamma} = 100$ s^{-1} the polymers remained in the coiled state, and extended at $\dot{\gamma} = 1000$ s^{-1} (see Fig. 5). It should

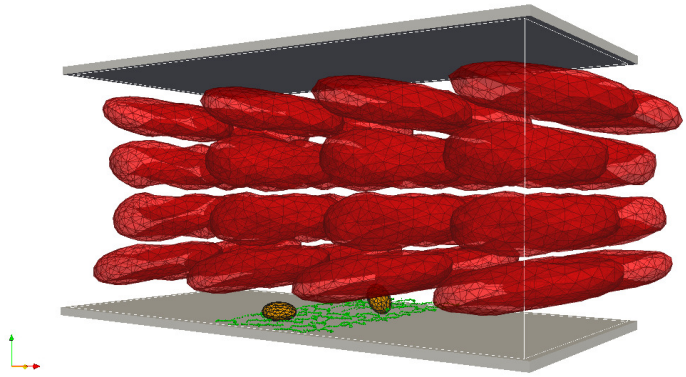

Figure 4. The simulation of the pressure-driven flow of the whole blood with hematocrit ≈ 0.3 for Reynolds number $\mathrm{Re} = 0.01$ in a $32 \times 16 \times 16\ \mu\mathrm{m}^3$ simulation box. The wall shear rate $\dot{\gamma} = 1000\ \mathrm{s}^{-1}$.

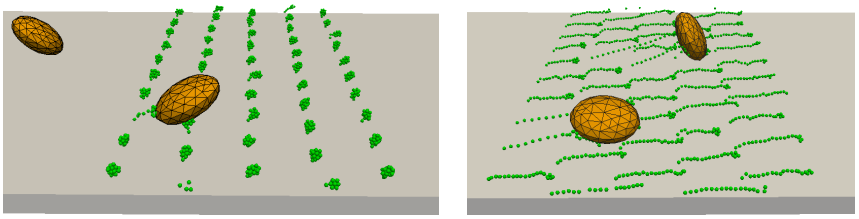

(a) (b)

Figure 5. The von Willebrand factor multimers change their conformation due to the increased shear rate in the near-wall fluid: (a) coiled (compact) conformation was observed for $\mathrm{Re} = 0.001$ ($\dot{\gamma} = 100\ \mathrm{s}^{-1}$) and (b) extended conformation — for $\mathrm{Re} = 0.01$ ($\dot{\gamma} = 1000\ \mathrm{s}^{-1}$).

be noted that the tethered polymers expand at smaller shear rates in the present model, in accordance with previous studies [6]. The extension of vWf multimers in response to the flow leads to the increased number of adhesive sites and should promote platelet aggregation. It is also noticeable that RBCs in the near-wall region move in a tank-treading pattern, which is a correct dynamics for these cells at high shear rates [20, 35].

3. Discussion and conclusions

In this work, a three-dimensional model for initial platelet adhesion to von Willebrand factor multimers has been presented. It has been shown through the comparison with the experiments that the chosen model on the chain-like polymer is valid for modelling the dynamics of vWf multimers at physiological shear rates. Possible future direction for the development of this model may include the precise tuning of the adhesion parameters, namely the amplitude of platelet–vWf interaction. Also, the catch–slip transition [30] that is typical for platelet membrane receptor GPIb,

which adheres to vWf, should be accounted for and added into the model. Other modifications may include more realistic inflow and outflow boundary conditions for platelets and vWf multimers (here periodic conditions were used), platelet activation, and optimization of the software.

A number of bio-mechanical effects related to the presence of red blood cells may have implications for the thrombosis. Blood rheology is probably the most notable one, as it depends on the cell–cell collisions and cell–fluid interactions. It has been shown earlier that in the microvasculature (arterioles and venules), where the typical wall shear rates are relatively high (> 500 s^{-1}), the Newtonian fluid is an adequate approximation for the blood rheology [21, 25, 44]. However, in veins and in stagnation regions, where the shear rates could be quite low (< 1 s^{-1}), the collisions and the adhesive interactions between the RBCs lead to the formation of rouleaux aggregates. This in turn increases the effective (apparent) viscosity of blood [19, 21]. This is why, probably, venous thrombi contain lots of RBCs, while arterial and microvascular thrombi consist mainly of platelets and fibrin [11]. Since the low-shear rate case was not the focus of the presented work, the aggregation of RBCs was not included into the reported model. Shear-thinning rheology of the whole blood could be, in principle, reproduced by LBM-DPD models [21], and it could be a fruitful direction of research in future.

The mechanics of red blood cells at high shear rates have important consequences not only for the rheology, but also for the distribution of cells across a blood vessel. The deformability of RBCs leads to the lift forces that repel the erythrocytes from the walls and gather them near the centerline of the vessel [9, 59]. It manifests as Fahraeus-Lindqvist effect and the formation of RBC depletion layer near the vessel wall [27, 46]. Another important phenomenon is the marginalization of blood platelets to the vicinity of the vessel wall. It has been demonstrated that the increased hematocrit causes the greater influx of the platelet to the injury or adhesive substrate [46, 51, 52]. There are at least two mechanisms that play role in this process: firstly, the margination of platelets causes the increase of their near-wall concentration [52], secondly, the RBCs collide with the platelets and push them to the vessel wall or the surface of a thrombus [46, 51]. Both effects promote thrombosis at the initial stages. However, it is not clear how the RBCs may change the dynamics of thrombosis during the latest stages of this process, when the stenosis becomes severe. In principle, it could be studied with the presented model in future.

References

1. P. Ahlrichs and B. Dunweg, Simulation of a single polymer chain in solution by combining lattice Boltzmann and molecular dynamics. *J. Chem. Physics* **111** (1999), No. 17, 8225–8239.
2. C. Aponte-Santamaria, V. Huck, S. Posch, A. K. Bronowska, S. Grässle, M. A. Brehm, T. Obser, R. Schneppenheim, P. Hinterdorfer, S. W. Schneider, C. Baldauf, and F. Gräter, Force-sensitive autoinhibition of the von Willebrand factor is mediated by interdomain interactions. *Biophys. J.* **108** (2015), 2312–2321.
3. N. Begent and G. V. R. Born, Growth rate in vivo of platelet thrombi, produced by iontophoresis of ADP, as a function of mean blood flow velocity. *Nature* **227** (1970), 926–930.

4. A. V. Belyaev, Hydrodynamic repulsion of spheroidal microparticles from micro-rough surfaces. *PLOS ONE* **12** (2017), No. 8, e0183093.

5. A. V. Belyaev, M. A. Panteleev, and F. I. Ataullakhanov, Threshold of microvascular occlusion: injury size defines the thrombosis scenario. *Biophys. J.* **109** (2015), 450–456.

6. A. V. Belyaev, Catching platelets from the bloodflow: the role of the conformation of von Willebrand factor. *Mat. Mod. Nat. Phenom.* **13** (2018), 44.

7. A. V. Belyaev, Long ligands reinforce biological adhesion under shear flow. *Phys. Rev. E* **97** (2018), 042407.

8. A. V. Belyaev, J. L. Dunster, J. M. Gibbins, M. A. Panteleev, and V. Volpert, Modelling thrombosis in silico: frontiers, challenges, unresolved problems and milestones. *Physics of Life Reviews* **26–27** (2018), 57–95.

9. N. Bessonov, E. Babushkina, S. Golovashchenko, A. Tosenberger, F. Ataullakhanov, M. Panteleev, A. Tokarev, and V. Volpert, Numerical simulation of blood flows with non-uniform distribution of erythrocytes and platelets. *Russian J. Numer. Anal. Math. Modelling* **28** (2013), 443–458.

10. M. Buš´ik and I. Cimrák, The calibration of fluid-object interaction in immersed boundary method. *EPJ Web of Conferences* **143** (2017), 02013.

11. J. R. Byrnes and A. S. Wolberg, Red blood cells in thrombosis. *Blood* **130** (2017), No. 16, 1795–1799.

12. A. Celi, G. Merrill-Skoloff, P. Gross, S. Falati, D. S. Sim, R. Flaumenhaft, B. C. Furie, and B. Furie, Thrombus formation: direct real-time observation and digital analysis of thrombus assembly in a living mouse by confocal and widefield intravital microscope. *J. Thrombosis Haemostasis* **1** (2002), 60–68.

13. H. Chen and A. Alexander-Katz, Structure and dynamics of blood-clotting-inspired polymer–colloid composites. *Soft Matter* **9** (2013), 10381.

14. S. Chen and C. D. Doolen, Lattice Boltzmann method for fluid flows. *Annual Review of Fluid Mechanics* **30** (1998), 329–364.

15. I. Cimrák, M. Gusenbauer, and I. Jančigová, An ESPResSo implementation of elastic objects immersed in a fluid. *Computer Physics Commun.* **185** (2014), No. 3, 900–907.

16. I. Cimrák and M. Gusenbauer and T. Schrefl, Modelling and simulation of processes in microfluidic devices for biomedical applications. *Computers Math. Appl.* **64** (2012), No. 3, 278–288.

17. C. Denis, N. Methia, P. S. Frenette, H. Rayburn, M. Ullman-Culleré, R. O. Hynes, and D. D. Wagner, A mouse model of severe von Willebrand disease: defects in hemostasis and thrombosis. *Proc. Nat. Acad. Sci. USA* **95** (1998), 9524–9529.

18. B. Dunweg and A. J. C. Ladd, Lattice Boltzmann Simulations of Soft Matter Systems. In: *Adv. in Polymer Sci.*, Springer, Berlin–Heidelberg, 2008.

19. T. L. Fabry, Mechanism of erythrocyte aggregation and sedimentation. *Blood* **70** (1987), No. 5, 1572–1576.

20. D. A. Fedosov, W. Pan, B. Caswell, G. Gompper, and G. E. Karniadakis. Predicting human blood viscosity in silico. *Proc. Nat. Acad. Sci. USA* **108** (2011), No. 29, 11772–11777.

21. D. A. Fedosov, M. Dao, G. E. Karniadakis, and S. Suresh, Computational bio-rheology of human blood flow in health and disease. *Ann. Biomed. Eng.* **42** (2014), 368–387.

22. M. H. Flamm, T. V. Colace, M. S. Chatterjee, H. Jing, S. Zhou, D. Jaeger, L. F. Brass, T. Sinno, and S. L. Diamond, Multiscale prediction of patient-specific platelet function under flow. *Blood* **120** (2012), 190–198.

23. A. L. Fogelson, Y. H. Hussain, and K. Leiderman, Blood clot formation under flow: the importance of factor XI depends strongly on platelet count. *Biophys. J.* **102** (2012), 10–18.

24. H. Fu, Y. Jiang, D. Yang, F. Scheiflinger, W. P. Wong, and T. A. Springer, Flow-induced elongation of von Willebrand factor precedes tension-dependent activation. *Nature Communications* **8** (2017), 324.

25. Y. C. Fung, *Biomechanics: Circulation.* Second edition. Springer-Verlag, New York, 1997.

26. B. Furie and B. C. Furie, Thrombus formation in vivo. *J. Clin. Invest.* **115** (2005), 3355–3362.

27. T. M. Geislinger and T. Franke, Hydrodynamic lift of vesicles and red blood cells in flow–from Fahraeus & Lindqvist to microfluidic cell sorting. *Advances in Colloid and Interface Science* **208** (2014), 161–176.

28. G. Giupponi, G. De Fabritiis, and Peter V. Coveney, Hybrid method coupling fluctuating hydrodynamics and molecular dynamics for the simulation of macromolecules. *J. Chemical Physics* **126** (2007), No. 15, 154903.

29. S. P. Jackson, W. S. Nesbitt, and E. Westein, Dynamics of platelet thrombus formation, *J. Thrombosis and Haemostasis* **7** (2009), No. 1, 17–20.

30. J. Kim, C.-Zh. Zhang, X. Zhang, and T. A. Springer, A mechanically stabilized receptor-ligand flex-bond important in the vasculature. *Nature* **466** (2010), 992–995.

31. M. J. Maxwell, E. Westein, W. S. Nesbitt, S. Giuliano, S. M. Dopheide, and S. P. Jackson, Identification of a 2-stage platelet aggregation process mediating shear-dependent thrombus formation. *Blood* **109** (2007), 566–576.

32. N. A. Mody and M. R. King, Platelet adhesive dynamics. Part I: characterization of platelet hydrodynamic collisions and wall effects, *Biophys. J.* **95** (2008), 2539–2555.

33. N. A. Mody and M. R. King, Platelet adhesive dynamics. Part II: high shear-induced transient aggregation via GPIba-vWF-GPIba bridging. *Biophys. J.* **95** (2008), 2556–2574.

34. D. Mori, K. Yano, K. Tsubota, T. Ishikawa, S. Wada, and T. Yamaguchi, Simulation of platelet adhesion and aggregation regulated by fibrinogen and von Willebrand factor. *Thromb. Haemost.* **99** (2008), 108–115.

35. L. Mountrakis, E. Lorenz, O. Malaspinas, S. Alowayyed, B. Chopard, and A. G. Hoekstra, Parallel performance of an IB-LBM suspension simulation framework. *J. Comput. Sci.* **9** (2015), 45–50.

36. J. P. Müller, S. Mielke, A. Löf, T. Obser, C. Beer, L. K. Bruetzel, D. A. Pippig, W. Vanderlinden, J. Lipfert, R. Schneppenheim, and M. Benoit, Force sensing by the vascular protein von Willebrand factor is tuned by a strong intermonomer interaction. *Proc. Nat. Acad. Sci.* **113** (2016), No. 5, 1208–1213.

37. L. Novák, Ha. Deckmyn, S. Damjanovich, and J. Hársfalvi, Shear-dependent morphology of von Willebrand factor bound to immobilized collagen. *Blood* **99** (2002), No. 6, 2070–2076.

38. I. V. Pivkin, P. D. Richardson, and G. Karniadakis, Blood flow velocity effects and role of activation delay time on growth and form of platelet thrombi. *Proc. Nat. Acad. Sci.* **103** (2006), No. 46, 17164–17169.

39. C. Pozrikidis, Orbiting motion of a freely suspended spheroid near a plane wall. *J. Fluid Mech.* **541** (2005), 105–114.

40. C. Pozrikidis, Flipping of an adherent blood platelet over a substrate. *J. Fluid Mech.* **568** (2005), 161–172.

41. K. Rack, V. Huck, M. Hoore, D. Fedosov, S. Schneider, and G. Gompper, Margination and stretching of von Willebrand factor in the blood stream enable adhesion. *Sci. Reports* **7** (2017), 14278.

42. D. A. Reasor, J. R. Clausen, and C. K. Aidun, Coupling the lattice-Boltzmann and spectrin-link methods for the direct numerical simulation of cellular blood flow. *Int. J. Numer. Methods Fluids* **68** (2012), No. 6, 767–781.

43. S. W. Schneider, S. Nuschele, A. Wixforth, C. Gorzelanny, A. Alexander-Katz, R. R. Netz, and M. F. Schneider, Shear-induced unfolding triggers adhesion of von Willebrand factor fibers. *Proc. Nat. Acad. Sci.* **104** (2007), 7899–7903.

44. R. Skalak, S. R. Keller, and T. W. Secomb, Mechanics of blood flow. *J. Biomech. Eng.* **103** (1981), 102–115.

45. H. Slayter, J. Loscalzo, P. Bockenstedt, and R. I. Handin, Native conformation of human von Willebrand protein. Analysis by electron microscopy and quasi-elastic light scattering. *J. Biological Chemistry* **260** (1985), No. 14, 8559–8563.

46. A. P. Spann, J. E. Campbell, S. R. Fitzgibbon, A. Rodriguez, A. P. Cap, L. H. Blackbourne, and E. S. G. Shaqfeh, The effect of hematocrit on platelet adhesion: experiments and simulations. *Biophys. J.* **111** (2016), 577–588.

47. T. A. Springer, Von Willebrand factor, Jedi knight of the bloodstream. *Blood* **124** (2014), No. 9, 1412–1425.

48. T. J. Stalker, E. A. Traxler, J. Wu, K. M. Wannemacher, S. L. Cermignano, R. Voronov, S. L. Diamond, and L. F. Brass, Hierarchical organization in the hemostatic response and its relationship to the platelet-signaling network. *Blood* **121** (2013), 1875–1885.

49. F. Storti, T. H. S. van Kempen, and F. N. van de Vosse, A continuum model for platelet plug formation and growth. *Int. J. Numer. Meth. Biomed. Eng.* **30** (2014), 634–658.

50. S. Succi, *The Lattice Boltzmann Equation for Fluid Dynamics and Beyond (Numerical Mathematics and Scientific Computation)*. Oxford University Press, USA, 2001.

51. A. A. Tokarev, A. A. Butylin, and F. I. Ataullakhanov, Platelet adhesion from shear blood flow is controlled by near-wall rebounding collisions with erythrocytes. *Biophys. J.* **100** (2011), 799–808.

52. A. A. Tokarev, A. A. Butylin, E. A. Ermakova, E. E. Shnol, G. P. Panasenko, and F. I. Ataullakhanov, Finite platelet size could be responsible for platelet margination effect. *Biophys. J.* **101** (2011), 1835–1843.

53. A. Tosenberger, F. Ataullakhanov, N. Bessonov, M. Panteleev, A. Tokarev, and V. Volpert. Modelling of thrombus growth in flow with a DPD-PDE method. *J. Theor. Biology* **337** (2013), 30–41.

54. R. Tran-Son-Tay, S. P. Sutera, and P. R. Rao, Determination of red blood cell membrane viscosity from rheoscopic observations of tank-treading motion. *Biophys. J.* **46** (1984), No. 1, 65–72.

55. W. Wang, N. A. Mody, and M. R. King, Multiscale model of platelet translocation and collision. *J. Comput Phys.* **244** (2013), 223–235.

56. W.-T. Wu, M. A. Jamiolkowski, W. R. Wagner, N. Aubry, M. Massoudi, and J. F. Antak, Multi-constituent simulation of thrombus deposition. *Sci. Reports* **7** (2017), 42720.

57. Z. Xu, N. Chen, S. C. Shadden, J. E. Marsden, M. M. Kamocka, E. D. Rosen, and M. Alber, Study of blood flow impact on growth of thrombi using a multiscale model. *Soft Matter* **5** (2009), 769–779.

58. A. Yazdani, H. Li, J. D. Humphrey, and G. E. Karniadakis, A general shear-dependent model for thrombus formation. *PLOS Computational Biology* **13** (2017), No. 1, e1005291.

59. H. Zhao and E. S. G. Shaqfeh, Shear-induced platelet margination in a microchannel. *Phys. Rev. E Stat. Nonlin. Soft Matter Phys.* **83** (2011), 061924.